JJMIE

Volume 9 Number 2, April.2015
ISSN 1995-6665
Pages 149 - 157

Jordan Journal of Mechanical and Industrial Engineering

Heatline Visualization of Buoyancy-Driven Flow inside a Nanofluid-Saturated Porous Enclosure

Iman Zahmatkesh*

Department of Mechanical Engineering, Mashhad Branch, Islamic Azad University, Mashhad, Iran

Received 15 Jan 2015 *Accepted 27 April 2015*

Abstract

In the present paper, the heatline visualization technique is utilized to understand heat transport path for buoyancy-driven flow inside a rectangular porous enclosure saturated with nanofluids. For this purpose, the mass, momentum and energy conservation equations are solved numerically adopting a control-volume based computational procedure. Moreover, the dimensionless heat function equation is utilized to determine the heat flow pattern inside the enclosure. Computations are undertaken for Cu, Al_2O_3, and TiO_2 nanoparticles in the base fluid of water and corresponding results in terms of dimensionless distributions of streamlines, isothermal lines, and heatlines as well as numerical values for flow strength and the average Nusselt number are compared with those of pure water under different Darcy-Rayleigh numbers. Additionally, the consequences of the nanoparticle fraction and the enclosure aspect ratio on the buoyancy-driven flow are analyzed. Inspection of the presented results indicates that among Cu-water, Al_2O_3-water, and TiO_2-water nanofluids, the Cu-water one produces higher heat transfer rates that is attributed to higher thermal conductivity of the Cu nanoparticles.

Keywords: *Nanofluid, Porous Media, Buoyancy-Driven Flow, Heatline, Enclosure*.

Nomenclature

AR	aspect ratio of the enclosure
Cv	constant-pressure specific heat
Da	Darcy number
g	gravitational acceleration
h	heat function
H	enclosure height
k	thermal conductivity
K	medium permeability
L	enclosure length
Nu	local Nusselt number
$\overline{Nu}$	average Nusselt number
Ra	Darcy-Rayleigh number
T	temperature
u,v	velocity components in x- and y-directions
x,y	Cartesian coordinates
X,Y	dimensionless coordinates

Greek symbols

α	thermal diffusivity
β	thermal expansion coefficient
θ	dimensionless temperature
μ	dynamic viscosity
π	dimensionless heat function
ρ	density
ϕ	nanoparticle fraction
ψ	stream function (m^2s-1)
Ψ	dimensionless stream function

Subscripts

bf	base fluid
C	cold
nf	nanofluid
p	nanoparticle

1. Introduction

Recent years have witnessed extensive research on convective heat transfer of nanofluids in the view of their abnormally better thermophysical properties. Thereby, it is not surprising to see some previous interests on the analysis of buoyancy-driven flow inside nanofluid-saturated porous enclosures. Sun and Pop [1], Chamkha and Ismael [2], Ahmed *et al.* [3], Rashidi *et al.* [4],

* Corresponding author. e-mail: zahmatkesh5310@mshdiau.ac.ir.

Bourantas *et al.* [5], Sheremet *et al.* [6], and Nguyen *et al.* [7] contributed some important findings in this field.

In spite of this, all the previous investigations on nanofluid-saturated porous enclosures were based on streamlines and isotherms. Although streamlines can adequately explain fluid flow, isotherms may not be sufficient for heat transfer analysis since heat flux lines are non-orthogonal to isotherms in a convection dominant regime. A more vigorous mean for the visualization of heat transfer in a two-dimensional convective transport process is provided by the distribution of heatlines. The concept of heatlines was introduced by Kimura and Bejan [8] as the trajectories of flow of heat energy and its use for visualization purposes is increasing (e.g., Saleh and Hashim [9-10], Basak *et al.* [11], and Rahman *et al.* [12]). The heatline visualization technique can be employed to observe not only path of heat flow but also intensity of heat flux at any location of domain for a convection heat transfer problem.

The objective of the present study is to visualize heat and fluid flow inside a nanofluid-saturated porous enclosure. For this purpose, streamlines, isothermal lines, and heatlines are obtained and plotted for enclosures saturated with Cu-water, Al_2O_3-water, or TiO_2-water nanofluids with different nanoparticle fractions, Darcy-Rayleigh numbers, and enclosure aspect ratios. Moreover, variations of the flow strength and the average Nusselt number with these parameters are presented. Based on the performed literature survey, this is the first study on the application of heat function on buoyancy-driven flows inside nanofluid-saturated porous enclosures.

2. Mathematical Formulation

An isotropic, homogenous, nanofluid-saturated porous enclosure is considered here with water as the base fluid. Figure 1 displays a schematic representation of this enclosure. Here, the left wall is heated and the right wall is cooled. Meanwhile, the horizontal walls are thermally insulated. The established flow is considered incompressible, Newtonian, and laminar. It is assumed that Local Thermal Equilibrium (LTE) exists between the nanofluid and the porous medium. The LTE is also assumed between the nanoparticles and the base fluid. The former is assumed here to be made up of Cu, Al_2O_3, or TiO_2. Except for the density in the body force term in the momentum equation for which the Oberbeck-Boussinesq approximation is adopted, thermophysical properties of the nanoparticles and the base fluid are kept constant with the numerical values reported in Table 1. The Darcy model, which assumes proportionality between velocity and pressure gradient, is used here to simplify the momentum equations. This model has been extensively used to study a number of fluid mechanics and heat transfer problems associated with fluid-saturated porous media (e.g., Duwairi *et al.* [13], Rashidi *et al.* [14]). With these assumptions, governing equations for continuity, momentum, and energy take the form of:

$$\frac{\partial u}{\partial \mathrm{x}}+\frac{\partial v}{\partial \mathrm{y}}=0, \tag{1}$$

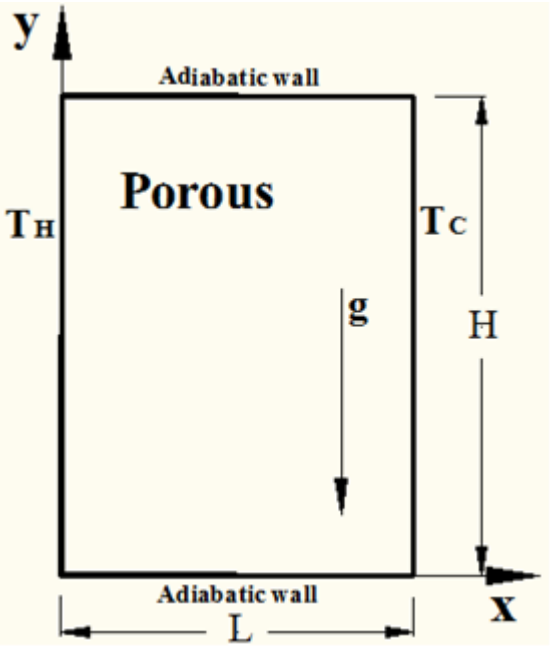

Figure 1. Schematic representation of the porous enclosure.

Table 1. Thermophysical properties of the nanoparticles and the base fluid at 300K.

Material	C_p $(Jkg^{-1}K^{-1})$	ρ (kgm^{-3})	k $(Wm^{-1}K^{-1})$	$\beta \times 10^{-5}$ (K^{-1})
Pure water	4179	997.1	0.613	21
Copper (Cu)	385	8933	401	1.67
Alumina (Al_2O_3)	765	3970	40	0.85
Titanium oxide (TiO_2)	686.2	4250	8.9538	0.9

$$u=-\frac{K}{\mu_{nf}}\frac{\partial p}{\partial x}, \tag{2}$$

$$v=\frac{Kg}{\mu_{nf}}\left[\phi\rho_p\beta_p+(1-\phi)\rho_f\beta_f-\phi(1-\phi)(\rho_p-\rho_f)(\beta_p-\beta_f)\right](T-T_C)-\frac{K}{\mu_{nf}}\frac{\partial p}{\partial y}, \tag{3}$$

$$u\frac{\partial T}{\partial x}+v\frac{\partial T}{\partial y}=\alpha_{nf}\left(\frac{\partial^2 T}{\partial x^2}+\frac{\partial^2 T}{\partial y^2}\right) \tag{4}$$

Here, *x* and *y* are the Cartesian coordinates while *u* and *v* are the velocity components in the *x*- and *y*-directions, respectively. *T* is the temperature, *K* is the medium permeability, *p* is the pressure, ρ is the density, μ is the dynamic viscosity, β is the thermal expansion coefficient, α is the effective thermal diffusivity, and ϕ is the nanoparticle fraction. In the equations above, the subscripts *p*, *f*, and *nf* stand for the nanoparticles, the base fluid, and the nanofluid, respectively.

The effective dynamic viscosity of the nanofluid is calculated from the Brinkman model [15]:

$$\mu_{nf} = \frac{\mu_f}{(1-\phi)^{2.5}}, \tag{5}$$

while the Maxwell-Garnetts model [16] is employed for the effective thermal conductivity:

$$\frac{k_{nf}}{k_f} = \frac{\left(k_p + 2k_f\right) - 2\phi\left(k_f - k_p\right)}{\left(k_p + 2k_f\right) + \phi\left(k_f - k_p\right)} \tag{6}$$

The effective thermal diffusivity of the nanofluid is defined as:

$$\alpha_{nf} = \frac{k_{nf}}{\rho_{nf}\, c_{p,nf}}, \tag{7}$$

with the heat capacitance of the nanofluid being in the form of:

$$\rho_{nf}\, c_{p,nf} = (1-\phi)\rho_f c_{p,f} + \phi\rho_p c_{p,p}. \tag{8}$$

Eliminating pressure terms in the momentum equations by applying cross-differentiation yields:

$$\frac{\partial u}{\partial y} - \frac{\partial v}{\partial x} = -\frac{Kg}{\mu_{nf}}\left[\phi\rho_p\beta_p + (1-\phi)\rho_f\beta_f - \phi(1-\phi)(\rho_p - \rho_f)(\beta_p - \beta_f)\right]\frac{\partial T}{\partial x}. \tag{9}$$

Introducing stream function (i.e., ψ) as:

$$u = \frac{\partial \psi}{\partial y}, v = -\frac{\partial \psi}{\partial x}, \tag{10}$$

automatically satisfies the continuity equation. Moreover, equations (4) and (9) take the form of

$$\frac{\partial^2 \psi}{\partial x^2} + \frac{\partial^2 \psi}{\partial y^2} = -\frac{Kg}{\mu_{nf}}\left[\phi\rho_p\beta_p + (1-\phi)\rho_f\beta_f - \phi(1-\phi)(\rho_p - \rho_f)(\beta_p - \beta_f)\right]\frac{\partial T}{\partial x} \tag{11}$$

and

$$\frac{\partial \psi}{\partial y}\frac{\partial T}{\partial x} - \frac{\partial \psi}{\partial x}\frac{\partial T}{\partial y} = \alpha_{nf}\left(\frac{\partial^2 T}{\partial x^2} + \frac{\partial^2 T}{\partial y^2}\right) \tag{12}$$

To obtain dimensionless governing equations, the following dimensionless variables are defined:

$$X = \frac{x}{L}, Y = \frac{y}{H}, AR = \frac{H}{L}, \Psi = \frac{\psi}{\alpha_f}, \tag{13}$$

$$\Theta = \frac{T - T_C}{T_H - T_C}, Ra = \frac{Kg\rho_f\beta_f(T_H - T_C)H}{\mu_f\alpha_f}$$

Here, *AR* is the enclosure aspect ratio and *Ra* is the Darcy-Rayleigh number.

Substituting equation (13) into equations (11) and (12) yields:

$$\frac{\partial^2 \Psi}{\partial X^2} + \frac{\partial^2 \Psi}{\partial Y^2} = -Ra(1-\phi)^{2.5}\left[(1-\phi) + \phi\left(\frac{\rho_p}{\rho_f}\right)\left(\frac{\beta_p}{\beta_f}\right) - \phi(1-\phi)\left(\frac{\rho_p}{\rho_f} - 1\right)\left(\frac{\beta_p}{\beta_f} - 1\right)\right]\frac{\partial \Theta}{\partial X} \tag{14}$$

$$\frac{\partial \Psi}{\partial Y}\frac{\partial \Theta}{\partial X} - \frac{\partial \Psi}{\partial X}\frac{\partial \Theta}{\partial Y} = \frac{\alpha_{nf}}{\alpha_f}\left[AR\frac{\partial^2 \Theta}{\partial X^2} + \frac{1}{AR}\frac{\partial^2 \Theta}{\partial Y^2}\right]. \tag{15}$$

The dimensionless boundary conditions for the problem at hand are:

$$X = 0, 0 < Y < 1: \Psi = 0, \Theta = 1, \tag{16a}$$

$$X = 1, 0 < Y < 1: \Psi = 0, \Theta = 0, \tag{16b}$$

$$0 < X < 1, Y = 0: \Psi = 0, \frac{\partial \theta}{\partial Y} = 0, \tag{16c}$$

$$0 < X < 1, Y = 1: \Psi = 0, \frac{\partial \Theta}{\partial Y} = 0. \tag{16d}$$

The local and the average Nusselt numbers at the hot (left) wall are calculated from the following expressions:

$$Nu = \frac{hH}{k_f} = -\frac{k_{nf}}{k_f} AR\left[\frac{\partial \Theta}{\partial X}\right]_{Y=0}, \tag{17}$$

$$\overline{Nu} = \int_0^1 Nu dY. \tag{18}$$

Heat Function

The heat function, defined by Kimura and Bejan [8], can be easily generalized to nanofluids problems as:

$$-\frac{\partial h}{\partial x} = \rho_{nf}\, c_{p,nf}\, v(T - T_C) - k_{nf}\frac{\partial T}{\partial y}, \tag{19}$$

$$\frac{\partial h}{\partial y} = \rho_{nf}\, c_{p,nf}\, u(T - T_C) - k_{nf}\frac{\partial T}{\partial x}, \tag{20}$$

With *h* being the heat function.

Adopting the dimensionless parameters defined by equation (13), the dimensionless form of equations (19) and (20) take the form of:

$$\frac{\partial \Pi}{\partial X} = \frac{\rho_{nf}\, c_{p,nf}}{\rho_f c_{p,f}}\theta\frac{\partial \Psi}{\partial X} + \frac{1}{AR}\frac{k_{nf}}{k_f}\frac{\partial \theta}{\partial Y}, \tag{21}$$

$$\frac{\partial \Pi}{\partial Y} = \frac{\rho_{nf}\, c_{p,nf}}{\rho_f c_{p,f}}\theta\frac{\partial \Psi}{\partial Y} - AR\frac{k_{nf}}{k_f}\frac{\partial \theta}{\partial X}, \tag{22}$$

where π is the dimensionless heat function:

$$\Pi = \frac{h}{k_f(T_H - T_C)}. \tag{23}$$

Assuming *h* to be a continuous function to its second-order derivatives, equations (21) and (22) lead to the following second-order differential equation for the dimensionless heat function:

$$\frac{\partial^2 \Pi}{\partial X^2} + \frac{\partial^2 \Pi}{\partial Y^2} = \frac{\rho_{nf}\, c_{p,nf}}{\rho_f c_{p,f}}\left[\frac{\partial}{\partial X}\left(\theta\frac{\partial \Psi}{\partial X}\right) + \frac{\partial}{\partial Y}\left(\theta\frac{\partial \Psi}{\partial Y}\right)\right] + \left(\frac{1}{AR} - AR\right)\frac{k_{nf}}{k_f}\frac{\partial^2 \theta}{\partial X \partial Y} \tag{24}$$

With this definition of the heat function, the positive sign of π denotes counter-clockwise heat flow while clockwise heat flow is represented by the negative sign of π.

The boundary conditions for the dimensionless heat function equation can be obtained from the integration of equations (21) and (22) along the enclosure boundary that yields:

$$0 < X < 1, Y = 0:\ \Pi(X,0) = \Pi(0,0) \quad (25a)$$

$$0 < X < 1, Y = 1: \Pi(X,1) = \Pi(0,1), \quad (25b)$$

$X = 0, 0 < Y < 1$:

$$\Pi(0,Y) = \Pi(0,0) - \int_0^Y AR\frac{k_{nf}}{k_f}\frac{\partial\theta}{\partial X}dY = \Pi(0,0) + \int_0^Y Nu.dY, \quad (25c)$$

$X = 1, 0 < Y < 1$:

$$\Pi(1,Y) = \Pi(1,0) - \int_0^Y AR\frac{k_{nf}}{k_f}\frac{\partial\theta}{\partial X}dY = \Pi(1,0) + \int_0^Y Nu.dY \quad (25d)$$

An important point in the determination of heat function goes back to its reference value. In this study, the value of heat function at the origin point is assumed to be $\pi(0, 0) = 0$.

Solution of equation (24) yields the values of the dimensionless heat function for the nodes inside the enclosure while drawing of the iso-lines of the heat function generates heatlines.

3. Solution Procedure

The resulting dimensionless partial differntial equations (equations (14), (15), and (24)) are solved simultaneously along with the corresponding boundary conditions (equations (16) and (25)). For this purpose, a control-volume based computational procedure is used. The governing equations are converted into a system of algebraic equations through integration over each control volume. The algebraic equations are solved by a line-by-line iterative method. The method sweeps the domain of integration along the *x* and *y* axes and uses Tri-Diagonal Matrix Algorithm (TDMA) to solve the system of equations. The employed FORTRAN code is essentially a modified version of a code built and validated in previous works [17-19]. The convergence criterion employed is the maximum residuals of all variables which must be less than 10^{-5}. To obtain a grid suitable for the range of Darcy-Rayleigh number studied here, a grid independence test is performed. It was observed that refinement of grid from 200 x 200 to 300 x 300 may not change the average Nusselt number values more than 1%. Thereby, a 200 x 200 grid is selected for the current computations.

4. Simulation Results

Since this is the first study on the application of heat function on buoyancy driven flows inside nanofluid-saturated porous enclosures, no previous results are available for the purpose of validation. Hence, the accuracy of the developed code is firstly tested with the classical natural convection heat transfer of pure fluid ($\phi = 0$) in a square porous enclosure with differentially-heated vertical walls and insulated horizontal walls. Accordingly, the obtained numerical values for the dimensionless temperature (ϕ) at the adiabatic walls are compared with those of Badruddin *et al.* [20] in Figure 2. As can be observed, current results are in excellent agreement with previously published works. Additionally, the validity of this solver, in the computation of nanofluid flows, is examined. For this purpose, natural convection heat transfer of Cu-water nanofluid in a triangular enclosure is computed and the obtained numerical values for the average Nusselt number are compared with those given by other authors in Table 2. As can be observed, current results are in excellent agreement with previously published works. Moreover, contour plots of stream function and temperature are almost the same as those reported in open literature. They are not, however, presented here for the sake of brevity. This provides confidence to the developed code for further studies. Consequently, in what follows, the code is utilized for the analysis of the nanofluid-saturated porous enclosure depicted in Figure 1.

Simulation results in terms of dimensionless distributions of streamlines (ψ), isothermal lines (θ), and heatlines π for Cu-water, Al_2O_3-water, and TiO_2-water nanofluids in a square porous enclosure (i.e., with *AR = 1*) are indicated in Figure 3 that corresponds to *Ra* = 10 and ϕ = 0.1. Here, the results of the pure water are also provided by the dashed lines for comparison. Moreover, numerical values of $|\Psi_{max}|$ and $\overline{Nu}$ for each case are illustrated.

Table 2. Comparison of the average Nusselt number in a nanofluid-saturated porous triangular enclosure with previously published works.

	Ra = 500		*Ra* = 1000	
	$\phi = 0$	$\phi = 0.2$	$\phi = 0$	ϕ =0.2
Sun and Pop [1]	9.66	9.42	13.9	12.85
Chamkha and Ismael [2]	9.52	9.44	13.6	12.82
Present study	9.53	9.41	13.67	12.81

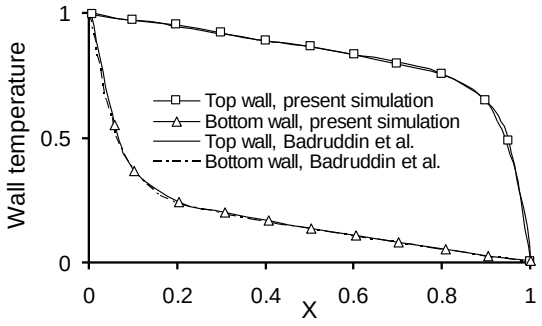

Figure 2. Computed adiabatic wall temperature compared with simulation results of Badruddin *et al.* [20].

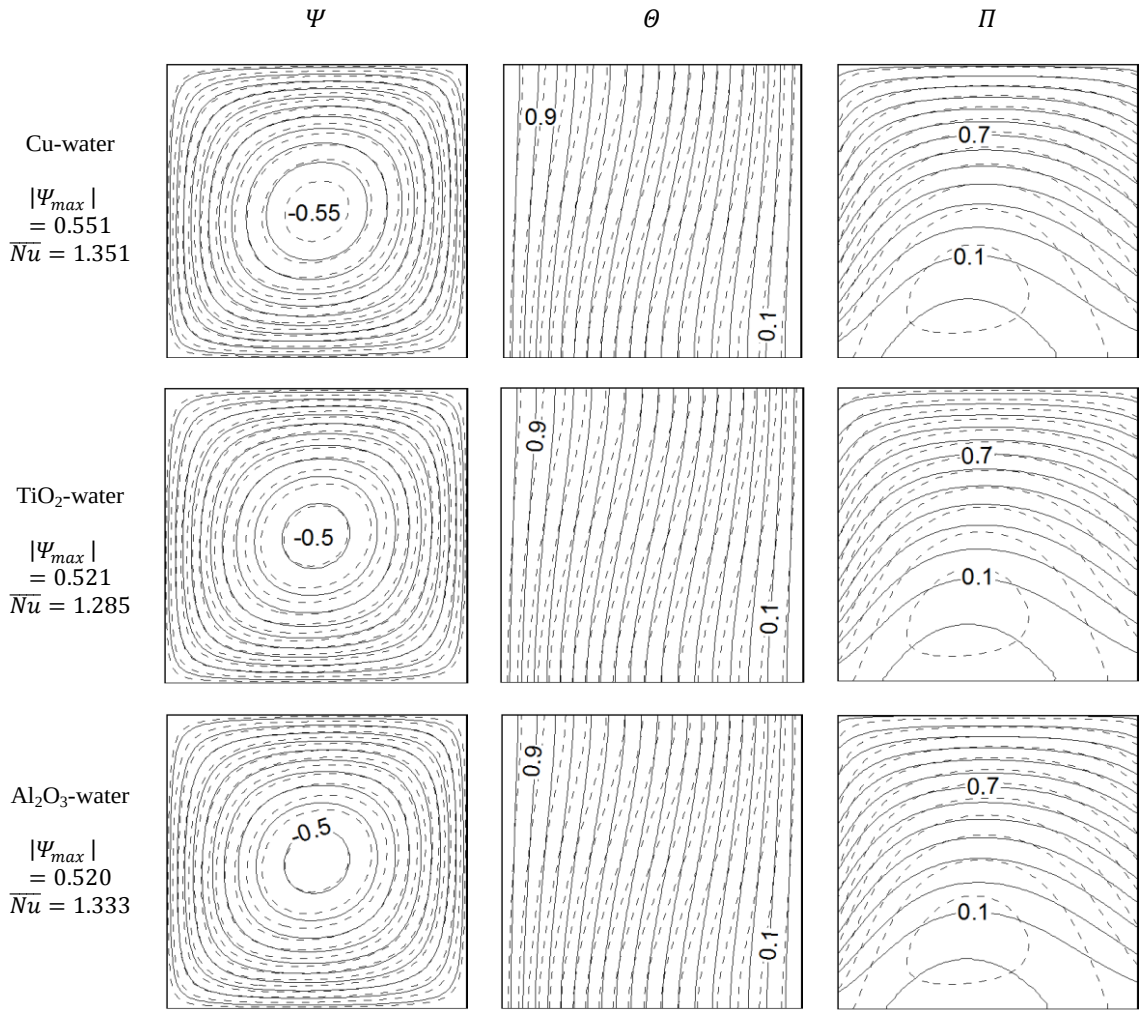

Figure 3. Distributions of streamlines, isothermal lines, and heatlines at $Ra = 10$ with $\phi = 0.1$ and $AR = 1$ (dashed lines correspond to pure water with $|\Psi_{max}| = 0.725$ and $\overline{Nu} = 1.067$).

The inspection of the streamlines as well as the isothermal lines demonstrates that close to the hot wall (i.e., the left wall), the fluid becomes heated and expands. This gives rise to an ascending motion. The fluid then changes its direction when reaching the neighborhood of the adiabatic wall. Thereafter, it releases heat at the cold wall (i.e., the right wall), becomes denser, and sinks down. These happenings result in the establishment of a closed-loop for fluid flow which transfers heat from the hot wall to the cold wall.

The combined effect of the fluid circulation and temperature distribution on the heat flow inside the enclosure is presented by the contour plots of heatlines. It is observed that heatlines emanate from hot wall and end on the cold wall implying the heat transport between the enclosure and its environment with no significant thermal mixing inside the enclosure.

The influence of nanoparticles on the buoyancy-driven flow is obvious. It is evident that with addition of the particles to the base fluid (i.e., water), the strength of the buoyancy-driven flow diminishes up to about 28%. Such an observation is in accord with the experimental evidence of Putra *et al.* [21] in non-porous environments and is attributed to the fact that densities of the current nanofluids are much higher than that of water. In spite of the observed decrease in $|\Psi_{max}|$, one may find up to about 27% increase in $\overline{Nu}$ with the particles addition. This is not a surprising effect due to the improvement of the thermal conductivity in this low-*Ra* environment.

To examine this behavior under different Darcy-Rayliegh numbers, the streamlines, isothermal lines, and heatlines for *Ra* = 100 and *Ra* = 1000 are plotted in Figures 4 and 5, respectively. Comparing the results of these figures with those in Figure 3 indicates that, at *Ra* = 10, the conduction heat transfer mechanism is dominant and the isotherms are nearly parallel to the vertical walls. The domination of conduction heat transfer in this low-*Ra* circumstance can also be observed in the heatline pattern since no passive area exists. It can be witnessed that with the increase in *Ra*, the flow strength enhances and thereby, the isotherms become gradually distorted. This also leads to the clustering of the heatlines from the hot to the cold wall and generates passive heat transfer area in which heat is rotated without having significant effect on heat transfer between the walls. Dense heatlines appearing in the vicinity of the mid parts of the vertical walls at *Ra* = 1000 depict higher heat transfer rates there. It is interesting to

observe that, with the increase in *Ra*, the pattern of the heatlines approaches to that of the streamlines; this is attributed to the domination of the convective mode of heat transport.

The inspection of the numerical values of $|\Psi_{max}|$ and $\overline{Nu}$ for the current nanofluids and those of pure water at $R_a = 100$ demonstrates up to about 16% decrease in $|\Psi_{max}|$ and up to about 15% decrease in $\overline{Nu}$ with the particles addition. At $Ra = 1000$; however, these diminishments take the values of 8% and 10%, respectively. This indicates that, with the increase in the Darcy-Rayleigh number, the effect of particles addition decreases.

Comparing the results of the current nanofluids leads one to conclude that the Cu-water nanofluid produces higher heat transfer rates in all circumstances. This is more clearly demonstrated in Figures 6 and 7 wherein the numerical values of the average Nusselt number for the three nanofluids in a wide range of nanoparticle fraction ($0 < \phi < 0.2$) and Darcy-Rayliegh number ($10 < Ra < 1000$) are provided. The physical reasoning for this behavior is the higher thermal conductivity of the Cu nanoparticles (see Table 1) and is in accord with the previous observations of Cho *et al.* [22].

Finally, the effect of enclosure aspect ratio on the buoyancy-driven flow is analyzed. To this aim, simulation results of $AR = 4$ are compared with those of $AR = 1$ in Figure 8. The presented results correspond to $Ra = 100$ and $\phi = 0.1$.

The influence of enclosure aspect ratio on the establishment of flow and thermal fields as well as heat transport path inside the enclosure is obvious. Comparing the numerical values of $|\Psi_{max}|$ and $\overline{Nu}$ in this Figure with those of Figure 4 indicates that with the increase in the enclosure aspect ratio, the strength of the buoyancy-driven flow decreases but the corresponding heat transfer rate enhances. The heat transfer enhancement occurs as a consequence of increase in the surface area of the non-adiabatic walls with respect to the adiabatic ones and is also observable from the dense heatlines in Figure 8. This is more clearly demonstrated in Figure 9 wherein the variations of the average Nusselt number with the enclosure aspect ratio for the current nanofluids are plotted. The figure indicates that in all of the analyzed enclosures, the Cu-water nanofluid produces higher heat transfer rates.

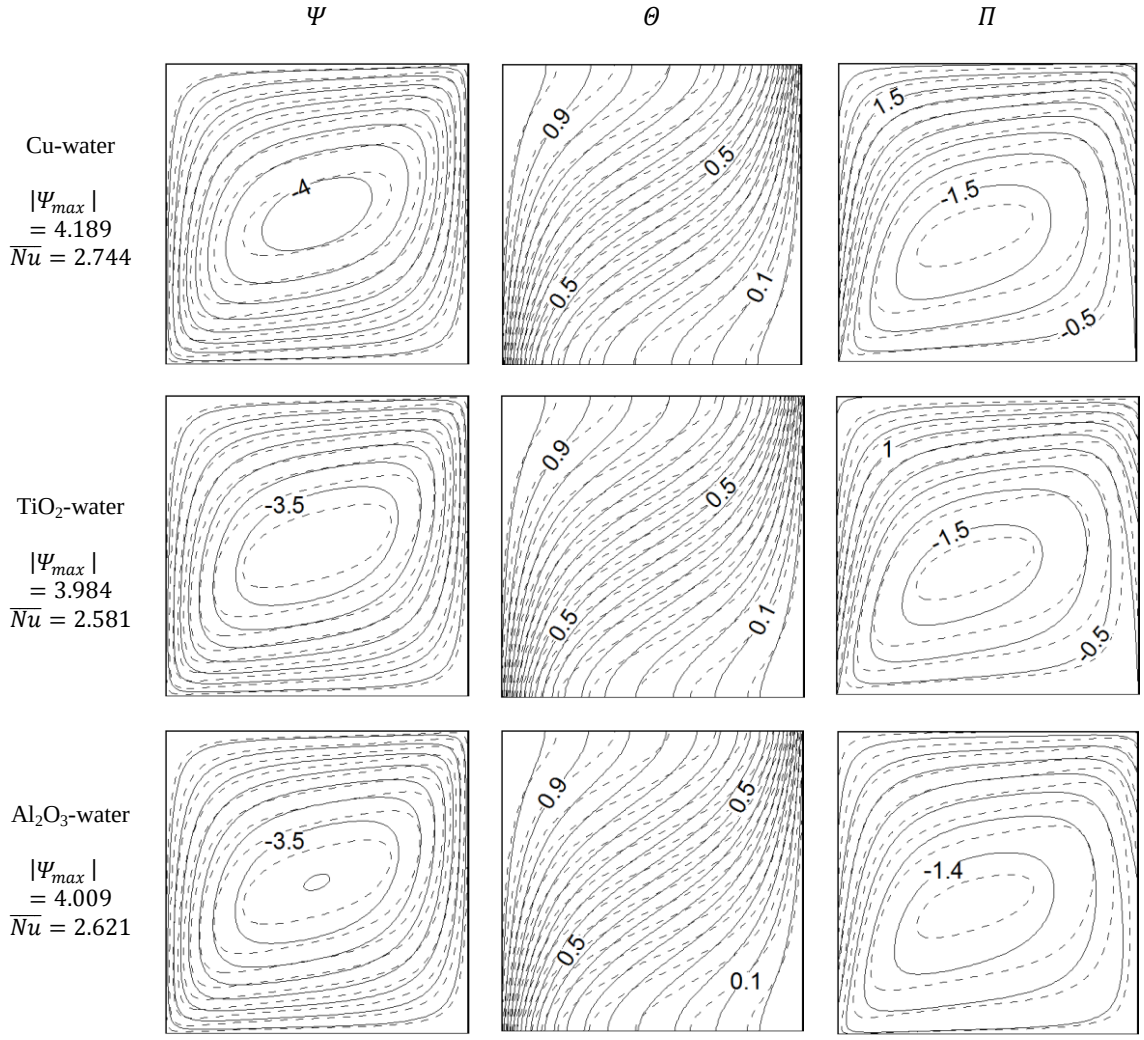

Figure 4. Distributions of streamlines, isothermal lines, and heatlines at $Ra = 100$ with $\phi = 0.1$ and $AR = 1$ (dashed lines correspond to pure water with $|\Psi_{max}| = 4.746$ and $\overline{Nu} = 3.025$).

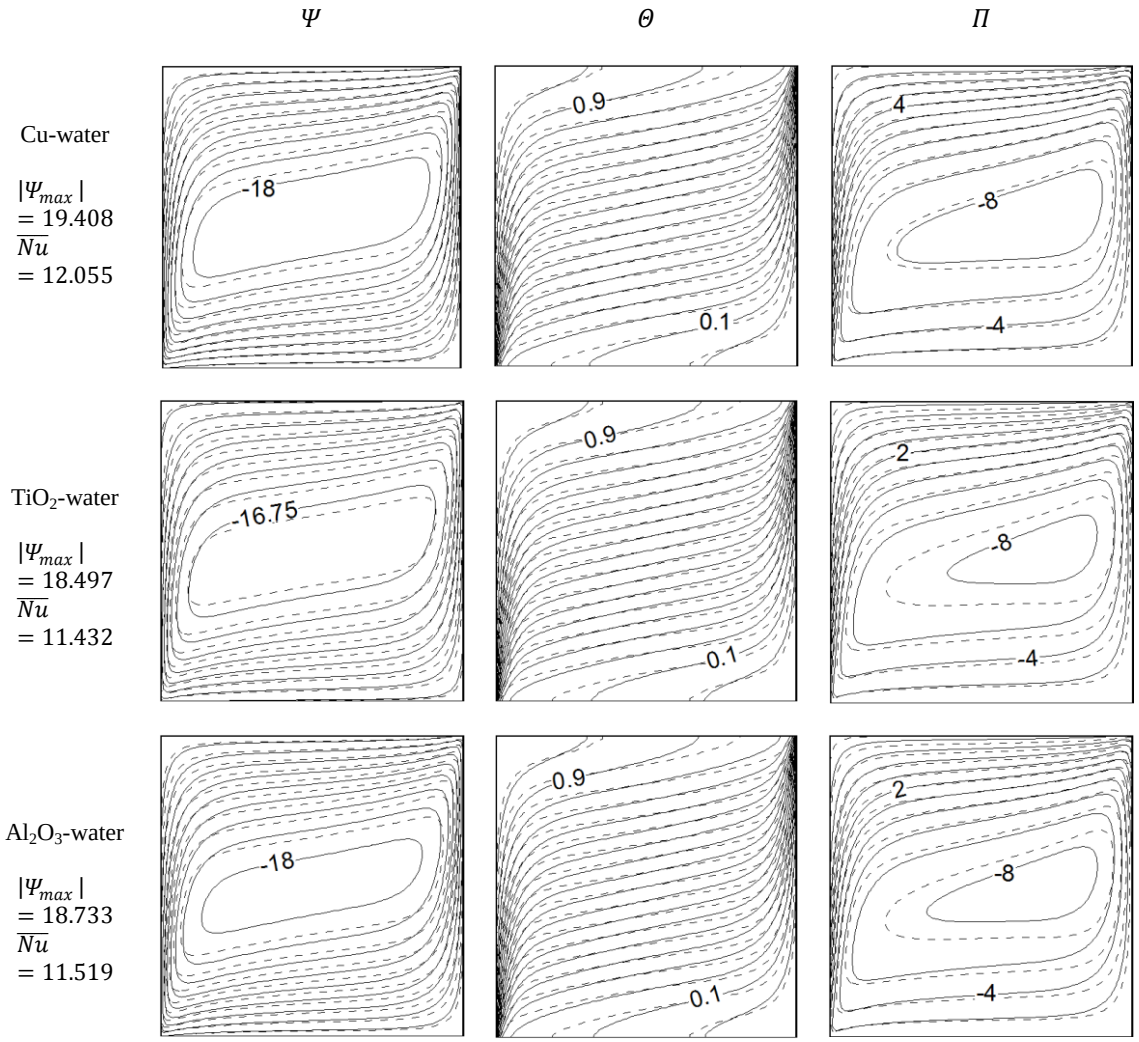

Figure 5. Distributions of streamlines, isothermal lines, and heatlines at $Ra = 1000$ with $\phi = 0.1$ and $AR = 1$ (dashed lines correspond to pure water with $|\Psi_{max}| = 20.071$ and $\overline{Nu} = 12.697$).

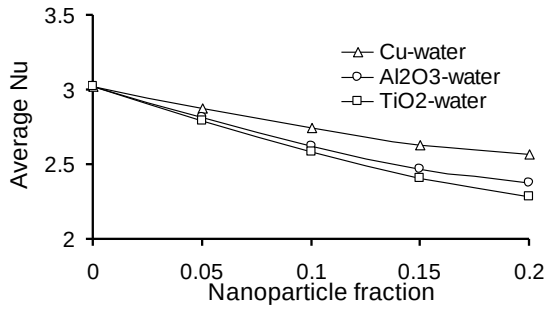

Figure 6. Variations of the average Nusselt number with nanoparticle fraction for the current nanofluids at $Ra = 100$

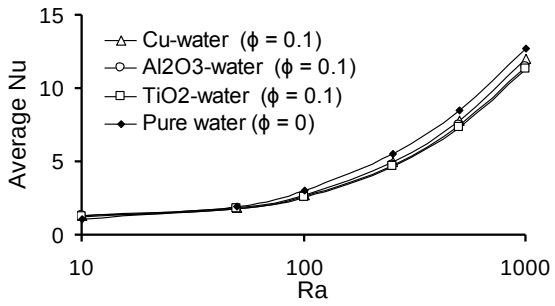

Figure 7. Variations of the average Nusselt number with Darcy-Rayliegh number for the current nanofluids with $\phi = 0.1$

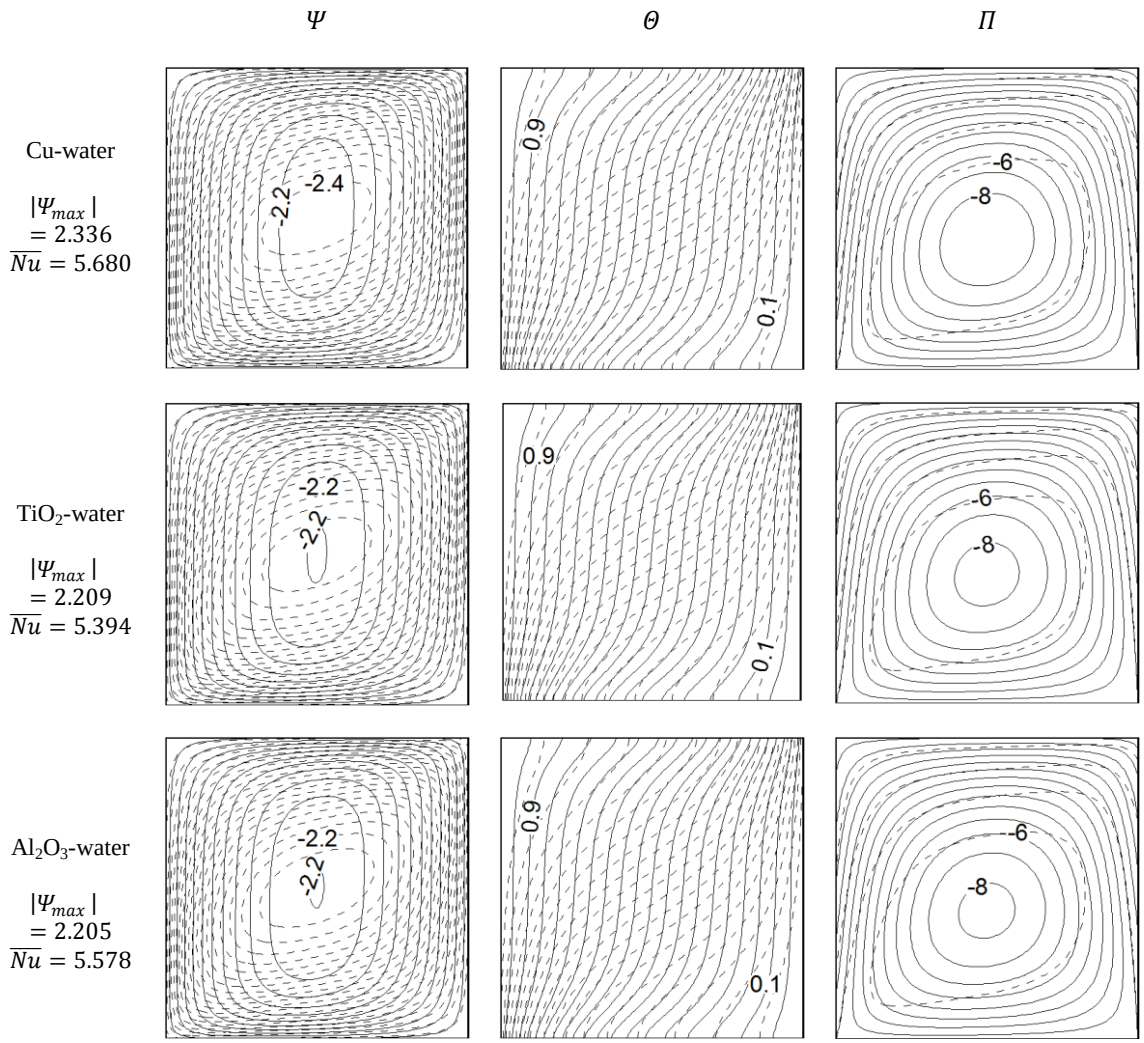

Figure 8. Distributions of streamlines, isothermal lines, and heatlines at $Ra = 100$ with $\phi = 0.1$ and $AR = 4$ (dashed lines correspond to the same nanofluid but with $AR = 1$).

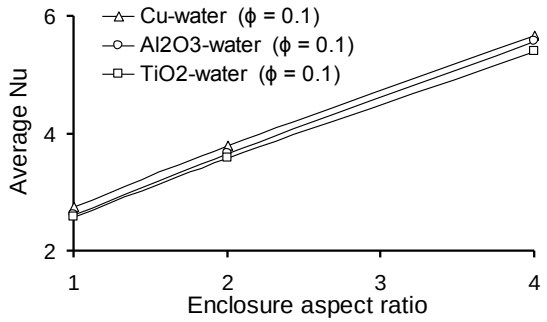

Figure 9. Effect of enclosure aspect ratio on the average Nusselt number at $Ra = 100$.

5. Concluding Remarks

The heatline visualization technique and its application to buoyancy-driven flow inside a nanofluid-saturated porous enclosure were discussed in the present study. Simulation results in terms of dimensionless distributions of streamlines, isothermal lines, and heatlines as well as numerical values of $|\Psi_{max}|$ and $\overline{Nu}$ for Cu-water, Al_2O_3-water, and TiO_2-water nanofluids were compared with those of pure water under different Darcy-Rayleigh numbers. Additionally, the consequences of the enclosure aspect ratio on the buoyancy-driven flow were clarified. Inspection of the presented results indicated how the establishment of the flow and thermal fields as well as the path of heat flow inside the enclosure may be influenced by the presence of the nanoparticles. It is found that among the current nanofluids, the Cu-water one produces higher heat transfer rates that is attributed to higher thermal conductivity of the Cu nanoparticles.

References

[1] Q. Sun, I. Pop, "Free convection in a triangle cavity filled with a porous medium saturated with nanofluids with flush mounted heater on the wall". International Journal of Thermal Sciences, Vol. 50 (2011) No. 11, 2141-2153.

[2] A.J. Chamkha, M.A. Ismael, "Conjugate heat transfer in a porous cavity filled with nanofluids and heated by a triangular thick wall". International Journal of Thermal Sciences, Vol. 67 (2013) 135-151.

[3] S.E. Ahmed, A.M. Rashad, R.S.R. Gorla, "Natural convection in triangular enclosures filled with nanofluid saturated porous media". Journal of Thermophysics and Heat Transfer, 27 (2013) No. 4, 700-706.

[4] M.M. Rashidi, E. Momoniat, M. Ferdows, A. Basiriparsa, "Lie group solution for free convective flow of a nanofluid past a chemically reacting horizontal plate in a porous media". Mathematical Problems in Engineering, Article ID 239082 (2014).

[5] G.C. Bourantas, E.D. Skouras, V.C. Loukopoulos, V.N. Burganos, "Heat transfer and natural convection of nanofluids in porous media". European Journal of Mechanics-B/Fluids, 43 (2014) 45-56.

[6] M.A. Sheremet, I. Pop, M.M. Rahman, "Three-dimensional natural convection in a porous enclosure filled with a nanofluid using Buongiorno's mathematical model". International Journal of Heat and Mass Transfer, Vol. 82 (2015) 396-405.

[7] M.T. Nguyen, A.M. Aly, W.W. Lee, "Natural convection in a non-Darcy porous cavity filled with Cu-water nanofluid using the characteristic-based split procedure in finite-element method". Numerical Heat Transfer, Part A, Vol. 67 (2015) No. 2, 224-247.

[8] S. Kimura, A. Bejan, "The "heatline" visualization of convective heat transfer". Journal of Heat Transfer, Vol. 105 (1983) No. 4, 916-919.

[9] H. Saleh, I. Hashim, "Heatline visualization of natural convection in an inclined square porous enclosure with sinusoidal boundary conditions". Journal of Porous Media, Vol. 16 (2013) No. 10, 875-885.

[10] H. Saleh, I. Hashim, "Heatline visualization of conjugate heat transfer in square porous enclosure". Journal of Porous Media, Vol. 16 (2013) No. 12, 1119-1132.

[11] T. Basak, A.K. Singh, T.P.A. Sruthi, S. Roy, "Finite element simulations on heat flow visualization and entropy generation during natural convection in inclined square cavities". International Communications in Heat and Mass Transfer, Vol. 51 (2014) 1-8.

[12] M.M. Rahman, H.F. Oztop, S. Mekhilef, R. Saidur, J. Orfi, "Simulation of unsteady heat and mass transport with heatline and massline in a partially heated open cavity". Applied Mathematical Modelling, Vol. 39 (2015) No. 5-6, 1597-1615.

[13] H.M. Duwairi, O. Abu-Zeid, R.A. Damesh, "Viscous and Joule heating effects over an isothermal cone in saturated porous media". Jordan Journal of Mechanical and Industrial Engineering, Vol. 1 (2007) No. 2, 113-118.

[14] M.M. Rashidi, O. Anwar Beg., N. Rahimzadeh, "A generalized differential transform method for combined free and forced convection flow about inclined surfaces in porous media". Chemical Engineering Communications, Vol. 199 (2012) No. 2, 257-282.

[15] H.C. Brinkman, "The viscosity of concentrated suspensions and solutions". Journal of Chemical Physics, Vol. 20 (1952) No. 4, 571-581.

[16] Maxwell J. A treatise on electricity and magnetism. 2nd ed. Cambridge: Oxford University Press; 1904.

[17] I. Zahmatkesh, "On the importance of thermal boundary conditions in heat transfer and entropy generation for natural convection inside a porous enclosure". International Journal of Thermal Sciences, Vol. 47 (2008) No. 3, 339-346.

[18] I. Zahmatkesh, "Dependence of buoyancy-driven flow inside an oblique porous cavity on its orientation". Emirates Journal for Engineering Research, Vol. 18 (2013) No. 2, 53-61.

[19] I. Zahmatkesh, "Effect of a thin fin on natural convection heat transfer in a thermally stratified porous layer". Emirates Journal for Engineering Research, Vol. 19 (2014) No. 2, 57-64.

[20] I.A. Badruddin, Z.A. Zainal, P.A.A. Narayana, K.N. Seetharamu, "Heat transfer in porous cavity under the influence of radiation and viscous dissipation". International Communications in Heat and Mass Transfer, Vol. 33 (2006) No. 4, 491-499.

[21] N. Putra, W. Roetzel, S.K. Das, "Natural convection of nano-fluids". Heat and Mass Transfer, Vol. 39 (2003) No. 8-9, 775-784.

[22] C.C Cho, C.L. Chen, C.K. Chen, "Natural convection heat transfer and entropy generation in wavy-wall enclosure containing water-based nanofluid". International Journal of Heat and Mass Transfer, Vol. 61 (2013) 749-758.